PCCP

View Online
Dynamic Article Links

Cite this: *Phys. Chem. Chem. Phys.*, 2011, **13**, 4679–4685

www.rsc.org/pccp

PAPER

A variable series resistance mechanism to explain the negative capacitance observed in impedance spectroscopy measurements of nanostructured solar cells

Juan Bisquert*

Received 16th November 2010, Accepted 5th January 2011
DOI: 10.1039/c0cp02555k

A simple model for conductivity modulation in a recombination diode is discussed to explain the observation of negative capacitance at forward bias observed in many optoelectronic devices. We formulate the basic recombination-modulation model in terms of an equivalent circuit for small ac perturbation and discuss the application of the results in measurements of impedance spectroscopy of dye-sensitized solar cells, organic solar cells and related systems.

1. Introduction

The impedance spectroscopy (IS) technique has been widely applied in nanostructured solar cells, such as dye-sensitized solar cells (DSC), quantum dot-sensitized solar cells, extremely thin absorber (eta) solar cells, and organic solar cells. While IS is a very useful tool for the characterization of these devices and for their physical understanding, in many cases an inductive loop is observed at very low frequencies.[1–5] This feature, associated with a negative capacitance, lacks a proper interpretation and causes great disconcert. This is furthermore not just an issue of purely academic interest. The negative capacitive feature intersects the determination of the device model and recombination mechanisms in the solar cells, and is therefore quite significant to foster the operation of the photovoltaic devices.

In recent years there has occurred a proliferation of observations of the negative capacitance, not only in the nanostructured solar cells, but in many types of organic and inorganic electronic and optoelectronic devices, such as organic and inorganic LEDs, for example.[5–12] Many explanations are specific to the particular system considered, and the discussions of the observed effects often use simulation tools based on complex device models. Sometimes explanations involve rather obscure physical considerations, or formal manipulations back and forth between time and frequency domains. In general the negative capacitance still remains a major problem in device physics.

From the wide variety of systems displaying negative capacitance reported in the literature, it can be expected that the physical mechanism of negative capacitance in different devices can be very different. However, it should be useful to define some broad criteria for the classification of the models. In Section 2 of this paper we describe a family of mechanisms based on the charge accumulation in an interfacial layer.

Another important strategy of explanation of the negative capacitance at forward bias is a feature of recombination diodes documented since the 1960s.[13–17] When a Schottky diode or a *pn* junction is forward biased, the amount of minority carriers injected increases exponentially with the bias potential. This causes a decrease of the series resistance (initially governed by majorities) that is known as conductivity modulation. In combination with the depletion or diffusion capacitance of the device, high level injection of minority carriers causes the impedance to turn to negative capacitance values. Explanations of conductivity modulation developed into specific models for *pn* junctions[18] or very sophisticated computer simulations.[19] The mechanism seems not to have received attention recently in the area of nanostructured solar cells and related devices. The main features of the negative capacitance observed in these systems are described in Section 3.

As mentioned above, in this field we need a simple physical picture that provides a suitable interpretation to the measured IS parameters. We cannot rely on full device model simulations since such models are not available and are even the object of investigation in many cases. Here, in Sections 4 and 5, I discuss a rather simple model of ac impedance of recombination diodes due to Barna and Horelick (BH).[14] This model captures the key aspect of the appearance of the negative capacitance by the reduction of a series resistance at forward bias. I present the implications of the model for the usual type of IS measurement: a small ac modulation under certain steady-state conditions. I show that this model provides a rather versatile mechanism that is likely to occur in nanostructured solar cells.

Grup de Dispositius Fotovoltaics i Optoelectrònics, Departament de Física, Universitat Jaume I, 12071 Castelló, Spain.
E-mail: bisquert@fca.uji.es

2. Overview of the intermediate layer model of negative capacitance

The inductive feature of the ac impedance is often found in electrochemical measurements of electrocatalytic reactions.[20–22] A scheme of these reactions is indicated in Fig. 1(a). The reaction A ⇔ C is controlled by an intermediate absorbed species B. In the domains of bias potential with negative capacitance (inductive behaviour) it is found that the concentration of the intermediate species departs strongly from equilibrium with the metal Fermi level.[22]

A similar mechanism occurs also in double-barrier resonant tunneling diodes (RTD), indicated in Fig. 1(b). In contradistinction to the basic concept of a parallel plate capacitor, the quantum capacitance was defined as the change of the charge stored in the quantum well with respect to a change of the potential in the RTD.[23] This concept is analogous to the chemical capacitance described below. It was shown that the quantum capacitance becomes negative in the region of negative differential resistance due to decrease of electron charges in the quantum well at increasing forward bias.[23–25]

Many electronic devices comprise a semiconductor between a rectifier contact and an ohmic contact, but with a layer of surface states or bulk traps where the charge storage and release can produce a large capacitive effect. A number of papers associated the negative capacitance with an interfacial layer or interfacial states in semiconductor devices.[26–29] This requires a mechanism whereby the interfacial states discharge under more injection, instead of accumulating more charge. For instance Evans *et al.* suggest an impact ionization model of the interface states.[26] Another model proposed for OLEDs is described in Fig. 1(c). Here the discharge of an interface state at the metal–polymer contact is caused by a shift of the surface energy levels.[30,31] A related effect is proposed in terms of free carriers in high resistivity materials[32] or trapped carriers[33] that accumulate close to one of the contacts (normally the rectifying contact).

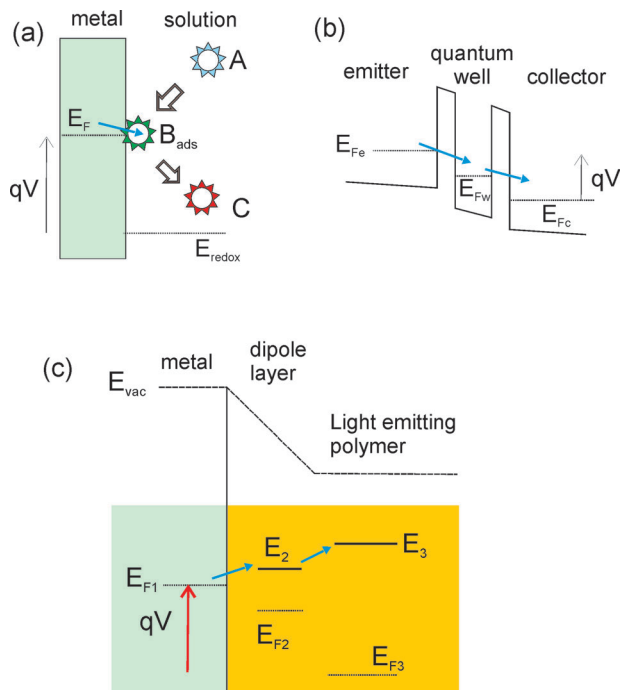

Fig. 1 (a) Scheme of an electrocatalytic reaction A ↔ C that requires an intermediate adsorbed species B_{ads}. The voltage V applied in the electrochemical cell relates to the difference between the metal Fermi level and the redox level in solution. (b) Scheme of a resonant-tunneling diode. The voltage applied in the diode relates to the difference of Fermi levels between the emitter and the collector. (c) Scheme of the electron injection at the organic/metal interface through a surface state in the dipole layer at the interface between the metal and a light-emitting polymer. Here the voltage produces both a rise of Fermi level in the metal contact and a change of the dipole layer potential.

Comparing the different mentioned systems, it is appreciated that the negative capacitance generally takes place when the current between two electronic reservoirs (such as bulk semiconductors, or ionic species in solution) is governed by the occupation of an intermediate state. In addition, it is found in the mentioned systems that the intermediate state occupation decreases when the applied potential increases. Therefore the occupation cannot be deduced from thermodynamic equilibrium arguments; a kinetic model is mandatory for describing the far from equilibrium state associated with the negative capacitance. In the RTD the negative capacitance is associated with a negative resistance as well (*i.e.*, a decrease of the current at forward bias). However in many semiconductor devices the negative capacitance exists in conjunction with exponentially increasing forward injection current (a positive recombination resistance).[26–29,32]

3. Experimental behaviour of negative capacitance in solar cells

Examples of negative capacitance in solar cells are reported in ref. 1–4 and 34. Some characteristic behaviours are shown in Fig. 2(a). In these measurements, the solar cell is set in the dark or at fixed illumination and the IS measurement is done at fixed bias potentials, from deep reverse to large forward bias (here taken as positive potential), past the open circuit voltage of the solar cell, which usually lies at +0.5–0.8 V. The impedance spectra are fitted to a model equivalent circuit (including inductive elements),[1] and the low frequency capacitance is determined.

In general, the capacitance of solar cells raises at forward bias, usually by the influence of the chemical capacitance.[35] The determination of the chemical capacitance at forward bias is a valuable tool for the analysis of the solar cell behaviour. For instance in dye solar cells the chemical capacitance of electrons in TiO_2 shows quantitatively the accumulation of electron carriers. Three examples of the "normal" exponentially raising capacitance are shown in Fig. 2(b), in DSCs with a liquid electrolyte, a viscous electrolyte, and the solid hole conductor OMeTAD.

The basic scheme of a solar cell is given in Fig. 3. Increasing the applied potential V_{app} in the forward direction produces an increase of the separation of the electron Fermi level E_{Fn} from the reference (equilibrium) level which is taken as the Fermi level of holes, E_{Fp}. The "Fermi level potential" is $V_F = (E_{Fn} - E_{Fp})/q$, q being the positive elementary charge.[36] Such internal potential and the applied bias differ, basically, by the series voltage drop

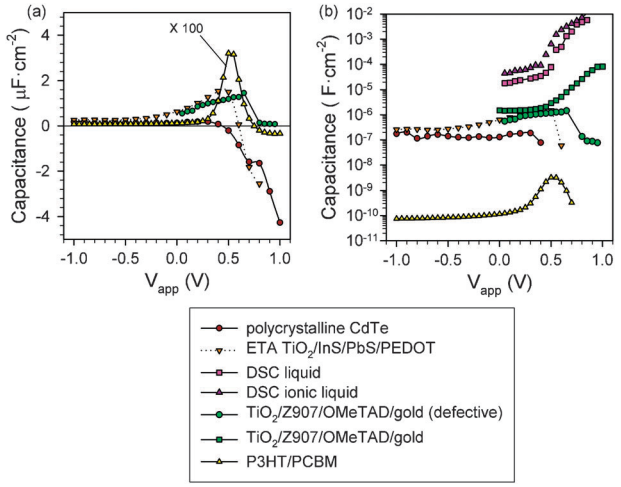

Fig. 2 (a) Characteristic results of solar cells showing negative capacitance at forward (negative) bias:[1,34] a polycrystalline CdTe solar cell, an extremely thin absorber (ETA) cell based on rough TiO_2, a dye-sensitized solar cell (defective) with the solid OMeTAD hole conductor, and a normal P3HT/PCBM bulk heterojunction organic solar cell. (b) The same data as in (a) in logarithmic scale, including the standard (positive) chemical capacitance of two dye-sensitized solar cells (nanostructured TiO_2/N719/iodide electrolyte) with both liquid and viscous electrolytes, and a regular DSC with the OMeTAD hole conductor.

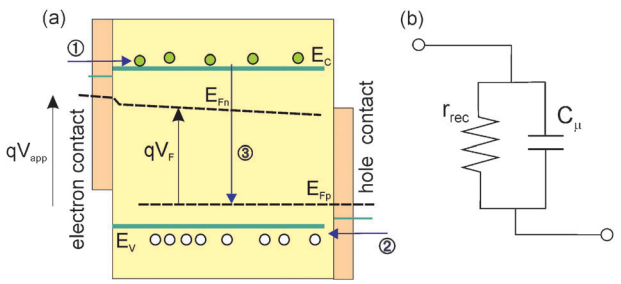

Fig. 3 (a) Energy diagram of a recombination diode consisting of a p-type semiconductor layer with electron selective contact at the left side and hole selective contact at the right side. q is the elementary charge, V_{app} is the voltage at the left terminal, E_c is the energy of the conduction band, E_v is the energy of the valence band, E_{Fn} is the electron Fermi level, E_{Fp} is the hole Fermi level, and V_F is the internal voltage associated with the separation of Fermi levels. The diode is shown at forward bias that injects electrons (1) and holes (2) what causes recombination (3). (b) The basic equivalent circuit for ac electrical perturbation. C_μ is the chemical capacitance of free (minority) carriers, r_{rec} is the recombination resistance of free carriers.

due to transport effects, see eqn (12) below. If the transport of minorities is efficient (by a sufficiently long diffusion length), E_{Fn} is close to homogeneous. On the other hand, if the semiconductor is poorly conducting in some region, strong inhomogeinities of carrier distribution occur.[32]

The chemical capacitance C_μ is generally defined in terms of the derivative of the number of minority carriers n with respect to the Fermi level potential,[35]

$$C_\mu = qL\frac{\mathrm{d}n}{\mathrm{d}V_F} \qquad (1)$$

Here L is the material thickness. For the case of Boltzmann statistics, the carrier number relates to the potential as

$$n = n_0 e^{qV_F/k_BT} \qquad (2)$$

where k_BT is the thermal energy and n_0 is an equilibrium density, and we obtain

$$C_\mu = \frac{q^2L}{k_BT}n = \frac{q^2Ln_0}{k_BT}e^{qV_F/k_BT} \qquad (3)$$

When E_{Fn} approaches the conduction band edge, the capacitance increases exponentially as a function of V_F.

Monitoring the increase of the chemical capacitance by IS (or related methods, such as charge extraction[37]) provides a picture of the raise of the Fermi level position across the active layer which is an important tool to establish a model of the solar cell operation. In addition, from a knowledge of the number of electrons as a function of the bias voltage, we can extract kinetic information about recombination, which allows explanation of the open-circuit voltage.[36–39]

The chemical capacitance displays a monotonic increase with the forward voltage (that represents the increasing Fermi level), as indicated in three examples in Fig. 2(b).[40,41] However in Fig. 2(a) a new effect appears that cannot be explained by the usual notion of a chemical capacitance in eqn (1). At a forward bias of $V_{appl} \approx +0.5$ V the capacitance starts to decrease, and at higher forward bias the capacitance becomes negative. This is seen for a polycrystalline CdTe cell, for a rough extremely thin absorber (ETA) cell,[1] and for a standard organic bulk heterojunction formed by a P3HT/P3BM.[34] For a (defective) DSC with the OMeTAD hole conductor,[42] the capacitance does not become negative but decreases to very low positive values due to the same type of effect. Further discussion about the experimental trends is given in ref. 34. In many materials the negative capacitance at forward bias can take values 100 times larger than the reverse (positive) saturation capacitance, or even much larger.[43]

The inconvenience of the presence of the negative capacitance is clear comparing the two OMeTAD cells in Fig. 2(b). By the effect of the negative capacitance we lose the connection of the measured capacitance with eqn (1), hence there is no information in the measured C about the accumulation of carriers, n, which we need for the interpretation of recombination and photovoltage, and in general to establish a solar cell device model. It is therefore necessary to obtain a suitable interpretation of the measured negative capacitance that provides access to relevant materials parameters.

4. The variable series resistance ac impedance model

We formulate the model in terms of the essential components of a nanostructured solar cell, as indicated in Fig. 3.[44] The elements in the equivalent circuit have the following interpretation. Injection of electron and holes creates a recombination current. We use the form of the diode model for the recombination current density

$$j_{rec} = j_d(e^{V_F/V_T} - 1) \qquad (4)$$

Here j_d is a constant parameter, the dark current (or "reverse saturation current"), and V_T is a parameter related to the thermal voltage that may include a diode quality factor m as follows:

$$V_T = \frac{mk_B T}{q} \tag{5}$$

We must mention that eqn (5) can be justified from the recombination rate expression

$$U = k_r p_0 n^{\beta} \tag{6}$$

Here k_r is the rate constant for recombination, p_0 is the constant density of majority carriers, and $\beta = 1/m$ is a generalized recombination order.[36,45] In the forward mode $V_F \gg V_T$, which is the only condition we consider here, we have

$$j_{rec} \propto U \propto n^{\beta} \tag{7}$$

It should be remarked here that recombination is a popular explanation of the negative capacitance. However ordinary recombination does not cause V_F to decrease when the current increases, as is evident from eqn (2) and (7), and an additional mechanism is necessary to obtain negative capacitance in the device.

The recombination resistance is given by

$$r_{rec} = \left(\frac{\partial j_{rec}}{\partial V_F}\right)^{-1} \approx \frac{V_T}{j_{rec}} \tag{8}$$

The approximation holds in the forward mode. The calculation of the impedance of this standard model[44] provides a simple expression

$$Z_a = \frac{1}{\frac{1}{r_{rec}} + i\omega C_\mu} \tag{9}$$

that corresponds to the parallel combination of r_{rec} and C_μ as shown in Fig. 3(b). In eqn (9) ω is the angular frequency of the ac perturbation.

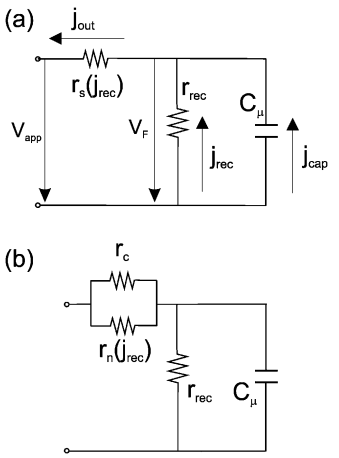

Fig. 4 (a) Equivalent circuit of the HB model for arbitrary voltage perturbation showing the branching of current and voltage in the recombination diode. (b) The series resistance contains two components in parallel.

To this standard model we add an essential component which is the series resistance as shown in Fig. 4(a). As mentioned in the Introduction, increasing the concentration of minority carriers in a *pn* junction diode reduces the conductivity along the diode material layer, so the series resistance decreases. In nanostructured solar cells, there is usually a combination of n and p-type materials and also limitations at the injecting/extracting contacts, and the origin of the series resistance is system-dependent to a large extent. The variable series resistance is described by BH in the following way

$$r_S = \left(\frac{1}{r_c} + \frac{1}{r_n}\right)^{-1} \tag{10}$$

The series resistance consists of two parallel components as shown in Fig. 4(b). r_c is a constant resistance and r_n describes a decrease of the series resistance. We assume as in BH:

$$r_n = \frac{V_{sd}}{j_{rec}} \tag{11}$$

Here V_{sd} is a constant parameter that controls the rate of the decrease of the series resistance with increasing current. The voltage applied in the diode has the form

$$V_{app} = V_F + j_{out} r_S \tag{12}$$

As shown in Fig. 4(a), the current in the outer circuit branches into two components: the recombination current and a current j_{cap} charging the chemical capacitor. Therefore

$$j_{out} = j_{rec} + j_{cap} \tag{13}$$

Furthermore the charging current can be written in the form

$$j_{cap} = C_\mu \frac{dV_F}{dt} = C_\mu \frac{dV_F}{dj_{rec}} \frac{dj_{rec}}{dt} = C_\mu r_{rec} \frac{dj_{rec}}{dt} \tag{14}$$

Note that the prefactor in the last expression of eqn (14) is the electron lifetime[46]

$$\tau_n = r_{rec} C_\mu \tag{15}$$

As usual in the calculation of impedance models we consider three types of quantities for each physical magnitude. The quantity with an overbar denotes a steady state condition, the quantity with a tilde is the amplitude of a small ac perturbation, and the quantity without marker denotes the general value. Thus

$$j_{out} = \bar{j}_{out} + \hat{j}_{out} \tag{16}$$

$$V_F = \bar{V}_F + \hat{V}_F \tag{17}$$

and so on.

Since we work in the frequency domain, eqn (14) gives the following relationship

$$\hat{j}_{cap} = i\omega\tau_n \hat{j}_{rec} \tag{18}$$

and from eqn (16)

$$\hat{j}_{out} = \hat{j}_{rec}(1 + i\omega\tau_n) \tag{19}$$

An expansion of eqn (4), using eqn (17) in the exponent, gives the following result

$$j_{\mathrm{rec}} = \bar{j}_{\mathrm{rec}}\left(1 + \frac{\hat{V}_{\mathrm{F}}}{V_{\mathrm{T}}}\right) \tag{20}$$

where $\bar{j}_{\mathrm{rec}}$ is given by eqn (4) at $\bar{V}_{\mathrm{F}}$, and we note that $\bar{j}_{\mathrm{out}} = \bar{j}_{\mathrm{rec}} = \bar{j}_{\mathrm{dc}}$. We have

$$\hat{j}_{\mathrm{rec}} = \bar{j}_{\mathrm{rec}}\frac{\hat{V}_{\mathrm{F}}}{V_{\mathrm{T}}} = \frac{\hat{V}_{\mathrm{F}}}{r_{\mathrm{rec}}} \tag{21}$$

and we obtain

$$\hat{j}_{\mathrm{out}} = \left(\frac{1}{r_{\mathrm{rec}}} + i\omega C_{\mu}\right)\hat{V}_{\mathrm{F}} \tag{22}$$

This result provides the external ac current as a linear function of the internal voltage. The calculation of the impedance is

$$Z = \frac{\hat{V}_{\mathrm{app}}}{\hat{j}_{\mathrm{out}}} \tag{23}$$

We need to make the linear expansion of $\hat{V}_{\mathrm{app}}$. However, we note that r_{S} depends on j_{rec}, so that it is required to find the dc and linear terms in r_{S}. The calculation is as follows

$$\begin{aligned} r_{\mathrm{S}} &= \left(\frac{1}{r_{\mathrm{c}}} + \frac{\bar{j}_{\mathrm{rec}} + \hat{j}_{\mathrm{rec}}}{V_{\mathrm{sd}}}\right)^{-1} \\ &= \bar{r}_{\mathrm{S}} - \frac{\bar{r}_{\mathrm{S}}^2}{V_{\mathrm{sd}}}\hat{j}_{\mathrm{rec}} \end{aligned} \tag{24}$$

where $\bar{r}_{\mathrm{S}}$ is r_{S} at $\bar{j}_{\mathrm{rec}}$. The negative term in eqn (24) is the crucial element producing the negative capacitance. From eqn (12)

$$V_{\mathrm{app}} = \left(\bar{j}_{\mathrm{out}} + \hat{j}_{\mathrm{out}}\right)\left(\bar{r}_{\mathrm{S}} - \frac{\bar{r}_{\mathrm{S}}^2}{V_{\mathrm{sd}}}\hat{j}_{\mathrm{rec}}\right) + \bar{V}_{\mathrm{F}} + \hat{V}_{\mathrm{F}} \tag{25}$$

and we have

$$\hat{V}_{\mathrm{app}} = \bar{r}_{\mathrm{S}}\,\hat{j}_{\mathrm{out}} - \frac{\bar{r}_{\mathrm{S}}^2 j_{\mathrm{dc}}}{V_{\mathrm{sd}}}\hat{j}_{\mathrm{rec}} + \hat{V}_{\mathrm{F}} \tag{26}$$

Using (22) and (26) in eqn (23) we obtain the expression of the impedance

$$Z_{\mathrm{b}} = \bar{r}_{\mathrm{S}} + \frac{B}{\frac{1}{\bar{r}_{\mathrm{rec}}} + i\omega\bar{C}_{\mu}} \tag{27}$$

where

$$B = 1 - \frac{\bar{r}_{\mathrm{S}}^2 j_{\mathrm{dc}}}{V_{\mathrm{sd}}} \tag{28}$$

which can be written also as

$$B = 1 - \frac{1}{V_{\mathrm{T}}V_{\mathrm{sd}}}\left(\frac{1}{V_{\mathrm{sd}}} + \frac{1}{r_{\mathrm{c}}j_{\mathrm{dc}}}\right)^{-2} \tag{29}$$

In general the model does not require the specific assumption of the series resistance in eqn (10) and (11). The appearance of negative capacitance requires that r_{S} decreases with the internal potential V_{F}. Eqn (27) for the impedance holds in the general case, and the coefficient is

$$B = 1 + j_{\mathrm{dc}}\frac{\mathrm{d}\bar{r}_{\mathrm{S}}}{\mathrm{d}\bar{V}_{\mathrm{F}}} \tag{30}$$

The critical current at which B becomes negative is

$$j_{\mathrm{c}} = -\left(\frac{\mathrm{d}\bar{r}_{\mathrm{S}}}{\mathrm{d}\bar{V}_{\mathrm{F}}}\right)^{-1} \tag{31}$$

which is also an old result in the conductivity modulation theory.[18]

5. Discussion

The final result of the HB model is given in eqn (27) and the equivalent circuit for the small ac perturbation is represented in Fig. 5(a). We see in eqn (27) that the fundamental RC parallel model of eqn (9) is naturally modified by the addition of the series resistance. But the exciting aspect is that Z_{a} impedance of eqn (9) is multiplied by a factor B which is negative at forward current $j_{\mathrm{dc}} > j_{\mathrm{c}}$. In this case the parallel connection of the Z_{a} model consists of a negative resistance Br_{rec} and negative capacitance $B^{-1}C_{\mu}$.

We should remark the reason for the change of circuit elements from Fig. 4(a) to Fig. 5(a). Fig. 4(a) shows a circuit valid for any kind of transient voltage, but r_{S} depends on the current through r_{rec}. Therefore if we apply the ac perturbation the element r_{S} in Fig. 4(a) is variable as indicated in eqn (24). Fig. 5(a) has another meaning. This circuit is valid for a small perturbation over a steady state. Here all the values in the equivalent circuit are set by the steady state value of voltage and current, and therefore the circuit elements do not depend on the amplitude or frequency of the perturbation. Thus Fig. 5(a) shows the appropriate equivalent circuit for the interpretation of the measurement of the IS technique.

The representation of the model of eqn (27) in terms of the equivalent circuit in Fig. 5(a) is not unique. One can transform the writing of the equation to provide other types of circuit

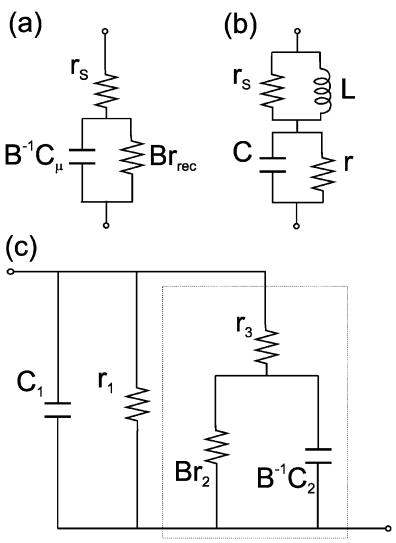

Fig. 5 Equivalent circuit for small ac perturbation (standard impedance spectroscopy measurements). (a) The model corresponding to eqn (27), (b) the equivalent circuit equivalent to (a) but in this case containing an inductor. (c) The model of (a) (in the box) with additional capacitance and resistance in parallel.

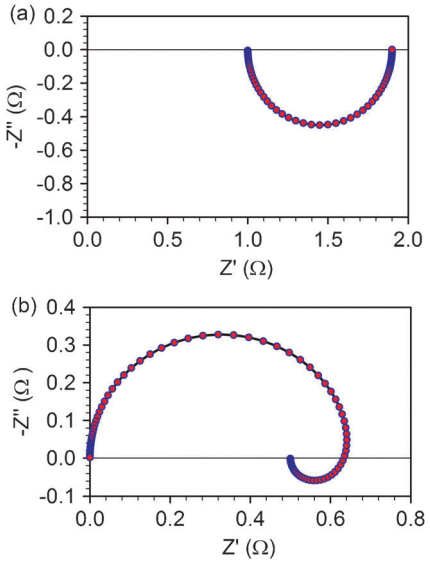

Fig. 6 Representation of the impedance in the complex plot. (a) The model of Fig. 5(a) for parameters $r_{rec} = 1\ \Omega$, $C_\mu = 1$ F, $B = -0.9$, $r_S = 1\ \Omega$. (b) Addition of parallel resistance ($r_1 = 1\ \Omega$) and capacitance ($C_1 = 0.1$ F) as in the model of Fig. 5(c).

representations. For example a manipulation of eqn (27) gives the following expression

$$Z_b = \frac{B + \frac{\bar{r}_S}{\bar{r}_{rec}}}{\frac{1}{\bar{r}_{rec}} + i\omega\bar{C}_\mu} + \frac{1}{\frac{1}{\bar{r}_S} + \frac{1}{i\omega\bar{r}_S\bar{r}_{rec}\bar{C}_\mu}} \qquad (32)$$

In this version the second term produces an inductive subcircuit containing the inductance $L = \bar{r}_S\bar{r}_{rec}\bar{C}_\mu$, as shown in Fig. 5(b). The equivalent circuit representation is a useful tool to interpret the measurements and one can choose the one that better suits this purpose. This is helpful and doesn't mean an indeterminacy of models. The model of eqn (27) is certainly unique and doesn't change depending on the way the formulas are written.

For the negative B values the model of eqn (27) produces an arc on the fourth quadrant of the impedance plot. This is shown in Fig. 6(a). In fact this impedance model was discussed in a recent publication,[47] in relation with recombination *via* semiconductor surface states by charge transfer of electrons to an acceptor in solution. In this model, formulated with a single type of electronic carrier, with standard trapping and recombination rates, the same equivalent circuit structure is obtained as in Fig. 5(a) but B remains positive.[47]

Comparing the surface states model[47] and the HB diode model discussed here, we remark that in the surface states model the series resistance is related to the exchange of carriers between the surface state and the conduction band in the semiconductor. Therefore, the parameter r_S in Fig. 5(a) can have very different physical origins in various situations.

If r_S actually displays the dependence in eqn (10) and (11), the range of negative values of B parameter is obtained for $V_{sd} < V_T$ and dc current of values $j_{dc} > j_c$ where

$$j_c = \frac{V_{sd}}{r_c}\frac{1}{\left(\frac{V_{sd}}{V_T}\right)^{1/2} - 1} \approx \frac{1}{r_c}(V_{sd}V_T)^{1/2} \qquad (33)$$

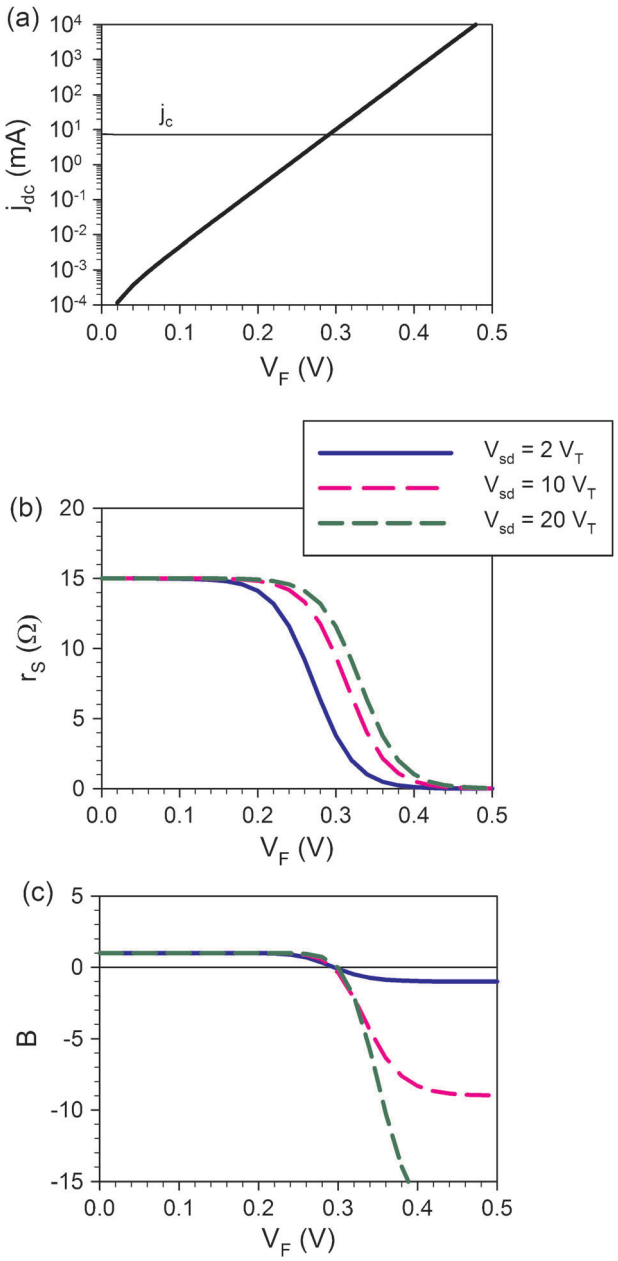

Fig. 7 Illustration of the model with parameters $j_d = 10^{-4}$ mA, $r_c = 15\ \Omega$, $V_T = 0.026$ V. (a) The diode current at forward bias as a function of internal potential. The critical current j_c is indicated. (b) Series resistance. (c) B parameter.

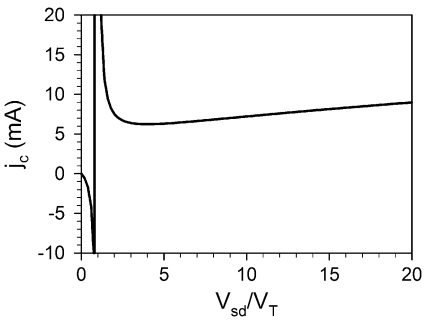

Fig. 8 Dependence of critical current on parameter V_{sd}.

An illustration of the model is shown in Fig. 7. The decrease of the series resistance shown in Fig. 5(b) causes a sudden drop of the B parameter, that becomes negative as seen in Fig. 7(c). This value is not very sensitive to the parameter V_{sd}, as is shown in Fig. 8. The main effect of changes of parameter V_{sd} occurs on the negative value of B, which grows very rapidly with forward bias voltage if V_{sd} is large.

According to our experience the spectrum of Fig. 6(a) is not observed in the measurement. In fact in nanostructured solar cells it is to be expected that the measured spectra contain contributions from other elements. Therefore we add to the model of eqn (27) a resistance and a capacitance in parallel, as indicated in Fig. 5(c). The resulting spectrum shown in Fig. 6(b) traces an arc formed (at high frequency) by r_1 and C_1 elements, that loops at low frequency to the fourth quadrant due to the negative components. This is indeed the shape of the characteristic spectra observed in measurements.[1–3] For the interpretation of Fig. 5(c) we may suggest that recombination in the solar cell is branched into two components: a direct component of electrons transferring to holes, and another branch mediated by some intermediate event. However to clarify the interpretation, application of the model to experimental situations will be needed. We believe these considerations will be useful to deal with the frequent presence of the inductive loop in nanostructured solar cells.

In conclusion, the model of HB allows us to develop a quantitative picture for the negative capacitance loop. The model provides a connection between the parameters determined at the equivalent circuit level. It is not claimed that conductivity modulation underlies all the observations of the negative capacitance at forward bias. In fact, the general structure of the equivalent circuit, in which the R and C elements in the parallel connection are affected by a B-factor, can be derived from quite different formulations. This simple picture can therefore be adapted to many situations using specific kinetic models.

Acknowledgements

I thank financial support from Ministerio de Ciencia e Innovación under project HOPE CSD2007-00007, and Generalitat Valenciana under project PROMETEO/2009/058.

References

1 I. Mora-Seró, J. Bisquert, F. Fabregat-Santiago, G. Garcia-Belmonte, G. Zoppi, K. Durose, Y. Y. Proskuryakov, I. Oja, A. Belaidi, T. Dittrich, R. Tena-Zaera, A. Katty, C. Lévy-Clement, V. Barrioz and S. J. C. Irvine, *Nano Lett.*, 2006, **6**, 640.
2 T. C. Li, M. S. Góes, F. Fabregat-Santiago, J. Bisquert, P. R. Bueno, C. Prasittichaia, J. T. Hupp and T. J. Marks, *J. Phys. Chem. C*, 2009, **113**, 18385.
3 I. Mora-Seró, S. Giménez, F. Fabregat-Santiago, R. Gomez, Q. Shen, T. Toyoda and J. Bisquert, *Acc. Chem. Res.*, 2009, **42**, 1848.
4 C. Lungenschmied, E. Ehrenfreund and N. S. Sariciftci, *Org. Electron.*, 2009, **10**, 115.
5 H. H. P. Gommans, M. Kemerink and R. A. J. Janssen, *Phys. Rev. B: Condens. Matter*, 2005, **72**, 235204.
6 H. C. F. Martens, J. N. Huiberts and P. W. M. Blom, *Appl. Phys. Lett.*, 2000, **77**, 1852.
7 I. N. Hulea, R. F. J. van der Scheer, H. B. Brom, B. M. W. Langeveld-Voss, A. van Dijken and K. Brunner, *Appl. Phys. Lett.*, 2003, **83**, 1246.
8 H. L. Kwok, *Solid-State Electron.*, 2003, **47**, 1089.
9 H. H. P. Gommans, M. Kemerink, G. G. Anderson and R. M. T. Pijper, *Phys. Rev. B: Condens. Matter*, 2004, **69**, 155216.
10 L. S. C. Pingree, B. J. Scott, M. T. Russell, T. J. Marks and M. C. Hersam, *Appl. Phys. Lett.*, 2005, **86**, 073509.
11 C. Y. Zhu, L. F. Feng, C. D. Wang, H. X. Cong, G. Y. Zhang, Z. J. Yang and Z. Z. Chen, *Solid-State Electron.*, 2009, **53**, 324.
12 E. Ehrenfreund, C. Lungenschmied, G. Dennler, H. Neugebauer and N. S. Sariciftci, *Appl. Phys. Lett.*, 2007, **91**, 012112.
13 W.-H. Ko, *Solid-State Electron.*, 1961, **3**, 59.
14 A. Barna and D. Horelick, *IEEE Trans. Circuit Theory*, 1971, **18**, 233.
15 M. A. Green and J. Shewchun, *Solid-State Electron.*, 1973, **16**, 1141.
16 J. Werner, A. F. J. Levi, R. T. Tung, M. Anzlowar and M. Pinto, *Phys. Rev. Lett.*, 1988, **60**, 53.
17 C. H. Champness and W. R. Clark, *Appl. Phys. Lett.*, 1990, **56**, 1104.
18 J. J. H. van den Biesen, *Solid-State Electron.*, 1990, **33**, 1471.
19 S. E. Laux and K. Hess, *IEEE Trans. Electron Devices*, 1999, **46**, 396.
20 M. T. M. Koper, *Adv. Chem. Phys.*, 1996, **92**, 1.
21 F. Berthier, J. P. Diard and C. Montella, *Electrochim. Acta*, 1999, **44**, 2397.
22 A. Sadkowski, *J. Electroanal. Chem.*, 1999, **465**, 119.
23 Y. Hu and S. P. Stapleton, *Appl. Phys. Lett.*, 1993, **58**, 167.
24 Y. Hu and S. P. Stapleton, *IEEE J. Quantum Electron.*, 1993, **29**, 327.
25 R. Lake and J. Tyang, *IEEE Trans. Electron Devices*, 2003, **50**, 785.
26 X. Wu, E. S. Tyang and H. L. Evans, *J. Appl. Phys.*, 1990, **68**, 2845.
27 E. Arslan, Y. Şafak, S. Altındal, O. Kelekçi and E. Özbay, *J. Non-Cryst. Solids*, 2010, **356**, 1006.
28 W. Z. Shen and A. G. U. Perera, *Appl. Phys. A*, 2001, **72**, 107.
29 F. El Kamel, P. Gonon, F. Jomni and B. Yangui, *Appl. Phys. Lett.*, 2008, **93**, 042904.
30 J. Bisquert, G. Garcia-Belmonte, A. Pitarch and H. Bolink, *Chem. Phys. Lett.*, 2006, **422**, 184.
31 G. Garcia-Belmonte, H. Bolink and J. Bisquert, *Phys. Rev. B: Condens. Matter*, 2007, **75**, 085316.
32 B. K. Jones, J. Santana and M. McPherson, *Solid State Commun.*, 1998, **107**, 47.
33 F. Lemmi and N. M. Johnson, *Appl. Phys. Lett.*, 1999, **74**, 251.
34 F. Fabregat-Santiago, G. Garcia-Belmonte, I. Mora-Seró and J. Bisquert, *Phys. Chem. Chem. Phys*, 2011, submitted.
35 J. Bisquert, *Phys. Chem. Chem. Phys.*, 2003, **5**, 5360.
36 E. M. Barea, C. Zafer, B. Gultein, B. Aydin, S. Koyuncu, S. Icli, F. Fabregat-Santiago and J. Bisquert, *J. Phys. Chem. C*, 2010, **114**, 19840.
37 R. Hamilton, C. G. Shuttle, B. O'Regan, T. C. Hammant, J. Nelson and J. R. Durrant, *J. Phys. Chem. Lett.*, 2010, **1**, 1432.
38 E. M. Barea, J. Ortiz, F. J. Payá, F. Fernández-Lázaro, F. Fabregat-Santiago, A. Sastre-Santos and J. Bisquert, *Energy Environ. Sci.*, 2010, **3**, 1985.
39 G. Garcia-Belmonte, P. P. Boix, J. Bisquert, M. Lenes, H. J. Bolink, A. La Rosa, S. Filippone and N. Martín, *J. Phys. Chem. Lett.*, 2010, **1**, 2566.
40 J. Bisquert, F. Fabregat-Santiago, I. Mora-Seró, G. Garcia-Belmonte, E. M. Barea and E. Palomares, *Inorg. Chim. Acta*, 2008, **361**, 684.
41 I. Mora-Seró, G. Garcia-Belmonte, P. P. Boix, M. A. Vázquez and J. Bisquert, *Energy Environ. Sci.*, 2009, **2**, 678.
42 M. S. Góes, F. Fabregat-Santiago, P. R. Bueno and J. Bisquert, *2009 MRS Fall Meeting Symposium R Proceedings*, 2010, **1211**, R0603.
43 C. D. Wang, C. Y. Zhu, G. Y. Zhang, J. Shen and L. Li, *IEEE Trans. Electron Devices*, 2003, **50**, 1145.
44 J. Bisquert and F. Fabregat-Santiago, *Dye-sensitized solar cells*, ed. K. Kalyanasundaram, CRC Press, Boca Raton, 2010.
45 J. Bisquert and I. Mora-Seró, *J. Phys. Chem. Lett.*, 2010, **1**, 450.
46 J. Bisquert, F. Fabregat-Santiago, I. Mora-Seró, G. Garcia-Belmonte and S. Giménez, *J. Phys. Chem. C*, 2009, **113**, 17278.
47 J. Bisquert, *J. Electroanal. Chem.*, 2010, **646**, 43.